

# The clustering of galaxies as a function of their photometrically-estimated atomic gas content

Cheng Li<sup>1\*</sup>, Guinevere Kauffmann<sup>2</sup>, Jian Fu<sup>2,1</sup>, Jing Wang<sup>2,3</sup>, Barbara Catinella<sup>2</sup>, Silvia Fabello<sup>2</sup>, David Schiminovich<sup>4</sup> and Wei Zhang<sup>5</sup>

<sup>1</sup>*Partner Group of the Max Planck Institute for Astrophysics and Key Laboratory for Research in Galaxies and Cosmology of Chinese Academy of Sciences, Shanghai Astronomical Observatory, Nandan Road 80, Shanghai 200030, China*

<sup>2</sup>*Max-Planck-Institute für Astrophysik, Karl-Schwarzschild-Str. 1, D-85741 Garching, Germany*

<sup>3</sup>*Department of Astronomy, University of Science and Technology of China, Jinzhai Road 96, Hefei 230026, China*

<sup>4</sup>*Department of Astronomy, Columbia University, 550 West 120th Street, New York, NY 10027, USA*

<sup>5</sup>*National Astronomical Observatories, Chinese Academy of Sciences, Beijing 100012, China*

Accepted ..... Received .....; in original form .....

## ABSTRACT

We introduce a new photometric estimator of the HI mass fraction ( $M_{\text{HI}}/M_*$ ) in local galaxies, which is a linear combination of four parameters: stellar mass, stellar surface mass density,  $NUV-r$  colour, and  $g-i$  colour gradient. It is calibrated using samples of nearby galaxies ( $0.025 < z < 0.05$ ) with HI line detections from the GASS and ALFALFA surveys, and it is demonstrated to provide unbiased  $M_{\text{HI}}/M_*$  estimates even for HI-rich galaxies. We apply this estimator to a sample of  $\sim 24,000$  galaxies from the SDSS/DR7 in the same redshift range. We then bin these galaxies by stellar mass and HI mass fraction and compute projected two point cross-correlation functions with respect to a reference galaxy sample. Results are compared with predictions from current semi-analytic models of galaxy formation. The agreement is good for galaxies with stellar masses larger than  $10^{10} M_\odot$ , but not for lower mass systems.

We then extend the analysis by studying the bias in the clustering of HI-poor or HI-rich galaxies with respect to galaxies with normal HI content on scales between 100 kpc and  $\sim 5$  Mpc. For the HI-deficient population, the strongest bias effects arise when the HI-deficiency is defined in comparison to galaxies of the same stellar mass and size. This is not reproduced by the semi-analytic models, where the quenching of star formation in satellites occurs by “starvation” and does not depend on their internal structure. HI-rich galaxies with masses greater than  $10^{10} M_\odot$  are found to be anti-biased compared to galaxies with “normal” HI content. Interestingly, no such effect is found for lower mass galaxies.

**Key words:** galaxies: clusters: general – galaxies: distances and redshifts – cosmology: theory – dark matter – large-scale structure of Universe.

## 1 INTRODUCTION

Over the past decade, large optical spectroscopic surveys such as the 2dF Galaxy Redshift Survey (2dFGRS; Colless et al. 2001) and the Sloan Digital Sky Survey (SDSS; York et al. 2000) have led to a resurgence in studies of the large scale structure of the Universe traced by galaxies. There are two main applications of such studies: a) to constrain cosmological parameters such as the matter density of the Universe  $\Omega_m$ , Hubble parameter  $h$ , fluctuation amplitude  $\sigma_8$  and neutrino mass in conjunction with constraints from other experiments, such as cosmic microwave

background (CMB) or Lyman  $\alpha$  forest measurements (e.g. Spergel et al. 2003; Tegmark et al. 2004; Eisenstein et al. 2005), b) to constrain models for the formation and evolution of the galaxy population.

Traditionally, large-scale structure studies that focus on cosmological applications aim to measure the clustering signal on large scales (tens of Mpc or greater). On large scales, the clustering amplitude depends only on the mass of the dark matter halos that host the galaxies. All galaxies, regardless of mass or type, trace the underlying dark matter density field in a simple linear fashion, so constraints on cosmological parameters are believed to be robust.

In contrast, studies aimed at constraining galaxy formation focus on the clustering signal on scales less than  $\sim 5$

\* E-mail: leech@shao.ac.cn

Mpc. On these scales, the clustering amplitude depends on not only the mass of the dark matter halos in which galaxies are found, but also the *location* of galaxies within their host halos (Benson et al. 2000; Peacock & Smith 2000).

In the current paradigm of galaxy formation within a merging hierarchy of dark matter halos, galaxies form when gas is able to cool, condense and form stars at the *centres* of dark matter haloes. At a later stage, the galaxy may be accreted into a larger dark matter halo and become a *satellite* galaxy in a group or a cluster. Gas is no longer supplied to these galaxies and star formation subsequently shuts down over some timescale (Kauffmann et al. 1993; Cole et al. 1994). In more recent models, gas is no longer supplied to central galaxies with central super-massive black holes located in dark matter halos containing a hot gas atmosphere (Croton et al. 2006; Bower et al. 2006).

One important goal in modern galaxy formation is to understand the physics behind these gas-related “accretion” and “quenching” processes in detail, because the timescales over which they operate and the way in which their efficiencies scale with halo and/or galaxy mass will determine how the galaxy population as a whole evolves as a function of cosmic epoch. Clustering analysis is a powerful tool in this endeavour. In particular, analysis of the *cross-correlation* between a specific galaxy sub-population and a larger “reference” sample allows one to maximize the  $S/N$  of the clustering measurement when the size of the sub-sample is small. This technique has recently been applied to sub-samples of narrow-line galaxies with actively accreting black holes in the SDSS to demonstrate that these galaxies are not triggered by mergers and are found preferentially at the centres of their dark matter haloes (Li et al. 2006b, 2008).

The clustering of galaxies as a function of their neutral gas content should in principle yield very interesting constraints on gas accretion and quenching processes in galaxies (e.g. Popping et al. 2009; Kim et al. 2011). Meyer et al. (2007) determined the two-point autocorrelation function (2PCF) of HI-rich galaxies using 4315 galaxies from the HI Parkes All Sky Survey (HIPASS; Zwaan et al. 2005) and found that HI selected galaxies exhibit weaker clustering than optically selected galaxies of the same luminosity. Recently Passmoor et al. (2011) measured the 2PCF for an early release of the Arecibo Legacy Fast ALFA (ALFALFA; Giovanelli et al. 2005) sample, finding similar results. The Meyer et al. (2007) study also looked at the dependence of clustering on total HI mass, finding it to be weaker than the dependence on both luminosity and on rotation velocity.

Up to now, there has been no attempt to study how clustering depends on HI mass *fraction* (i.e.  $M_{HI}/M_*$ ), a quantity that ought to be much more directly related to accretion and quenching processes that affect the gas content of a galaxy, but not its stellar mass. In addition, a power-law form for the correlation function has been *assumed* in these previous clustering analyses, which means that information about location of the galaxies within their dark matter haloes (alternatively central or satellite galaxy fraction), cannot be recovered. Finally, because available samples are small, it has not been possible to study clustering as a function of HI mass fraction in conjunction with other galaxy parameters, such as stellar mass or stellar surface mass density. In this work we will demonstrate how an approach that combines HI data for a small, but complete sample of 1000 galaxies

and optical data for a much larger sample of galaxies from the SDSS Data Release 7 (DR7; Abazajian et al. 2009) can be used to study the influence of dark matter halo mass and environment on the gaseous properties of galaxies.

The GALEX Arecibo SDSS Survey (GASS; Catinella et al. 2010) is measuring the atomic gas content of a sample of  $\sim 1000$  galaxies with redshifts and stellar masses in the ranges  $0.025 < z < 0.05$  and  $10^{10} < M_* < 10^{11.5} M_\odot$ . Each galaxy is observed until the HI line is detected or until an upper limit of  $\sim 0.015$  in the atomic-to-stellar mass ratio is reached. The GASS galaxies are selected from the SDSS spectroscopic and Galaxy Evolution Explorer (GALEX; Martin et al. 2005), so stellar masses, sizes and structural parameters are available from the MPA/JHU data base (<http://www.mpa-garching.mpg.de/SDSS/>). The scaling relations of the HI mass fraction of the GASS galaxies ( $M_{HI}/M_*$ ), as a function of global galaxy parameters such as stellar mass  $M_*$ , surface mass density  $\mu_*$ , light concentration index  $C$  (defined as  $R_{90}/R_{50}$ , the ratio of the radii enclosing 90 and 50 percent of the total  $r$ -band light) and specific star formation rate  $SFR/M_*$  are presented in Catinella et al. (2010, hereafter C10) and Schiminovich et al. (2010).

Following the work of Zhang et al. (2009), C10 defined a gas-fraction “plane” linking HI mass fraction, stellar surface mass density and  $NUV - r$  colour that exhibited a scatter of 0.315 dex in  $\log_{10} M_{HI}/M_*$ , considerably tighter than the relation between HI mass fraction and optical/near-IR colour studied by Kannappan (2004), which had a scatter of  $\sim 0.4$  dex. The improvement in scatter indicates that the HI content of a galaxy scales with its physical size as well as with its star formation rate. In subsequent work, Wang et al. (2011) showed that at fixed  $NUV - r$  colour and stellar surface density, galaxies with larger HI gas fractions have bluer outer disks.

In this paper, we include the *colour gradient* of galaxies as an additional parameter in our fits. This produces a relation with similar scatter, but that better predicts the HI mass fraction of the most gas-rich galaxies in our samples. We use this relation to predict the HI content of the galaxies in our SDSS/DR7 sample. We then study how clustering depends on both “pseudo” HI mass fraction, and a “pseudo” HI excess/deficiency parameter, which we define as the deviation in the predicted HI content of a galaxy from the average HI content of all galaxies of the same stellar mass and surface mass density. This “pseudo” HI excess/deficiency parameter depends on a combination of  $NUV - r$  colour and  $g - i$  colour gradient. Finally, we compare our results with clustering predictions from the semi-analytic galaxy formation models of Fu et al. (2010, hereafter F10) and Guo et al. (2011, hereafter G11). The main way in which the F10 model differs from the G11 model is that it includes simple prescriptions for molecular gas formation processes.

The motivation behind expressing the results in this paper in terms of “pseudo” HI fraction, rather than in terms of directly measured photometric quantities, is because this provides insight into physical processes regulating the gas supply in galaxies. The semi-analytic models make a host of assumptions about how gas is accreted from the surround dark matter halo and then consumed into stars. By comparing clustering as a function of gas fraction in the models with the data, we hope to ascertain whether these assumptions

are correct, or whether there are discrepancies that warrant further investigation.

Throughout this paper we have assumed a cosmology with  $\Omega = 0.3$ ,  $\Lambda = 0.7$  and  $H_0 = 70 \text{ km s}^{-1} \text{ Mpc}^{-1}$  when computing observed quantities. A Hubble constant of  $H_0 = 100 \text{ km s}^{-1} \text{ Mpc}^{-1}$  is assumed when presenting correlation function measurements. We note that the F10 and G11 models are based on simulations with  $\Omega = 0.25$  and  $\Lambda = 0.75$ . This will make a small difference in the comparison between data and models. We note that the focus of this paper is not on obtaining precision fits to the data, but on identifying major discrepancies that may lead us to change the input physics in the model.

## 2 DATA

### 2.1 GASS galaxy sample

The parent sample of GASS consists of 12,006 galaxies selected from the region of sky where the sixth data release (DR6; Adelman-McCarthy et al. 2008) of the SDSS overlaps the maximal ALFALFA footprint. All galaxies are selected to have stellar masses  $M_* > 10^{10} M_\odot$  and redshifts in the range  $0.025 < z < 0.05$ . The GASS sample is constructed by randomly selecting a subset of  $\sim 1000$  galaxies from the parent sample within the footprint of the GALEX Medium Imaging Survey so that the distribution in stellar mass is flat. The targets are observed with the Arecibo radio telescope until detected or until an H I mass fraction  $M_{\text{HI}}/M_*$  limit of 1.5-5 per cent is reached. In this work, we use the *representative* sample of 480 GASS galaxies, including 293 detections and 187 non-detections described in Catinella et al. (2011). Details of the GASS survey design, target selection and observing procedures can be found in C10.

### 2.2 SDSS galaxy samples

We have constructed two galaxy samples from the SDSS/DR7.

The first sample, which will serve as our *reference* sample in the clustering analysis, is a magnitude-limited sample of 66,461 galaxies with  $r < 17.6$ ,  $-24 < M_{0.1r} < -16$  and redshifts in the range  $0.025 < z < 0.05$ . Here,  $r$  is the  $r$ -band Petrosian apparent magnitude, corrected for Galactic extinction, and  $M_{0.1r}$  is the  $r$ -band Petrosian absolute magnitude, corrected for evolution and  $K$ -corrected to its value at  $z = 0.1$ . These selection criteria, with the exception of the redshift range, are the same as in our previous papers where we studied the clustering of galaxy luminosity and stellar mass (e.g. Li et al. 2012). We have generated *random* samples that have the same sky coverage as well as the same position- and redshift-dependent selection effects as the reference sample. Details of this procedure are presented in our previous papers (e.g. Li et al. 2006a).

The second sample contains 36,136 galaxies, and is a subset of the reference galaxies with stellar masses in the range  $10^{9.5} M_\odot < M_* < 10^{11} M_\odot$ . In the next section we will estimate an H I mass fraction for each galaxy in this sample using our newly calibrated photometric estimator. We select a number of subsamples binned according to  $M_*$  and

$M_{\text{HI}}/M_*$ , and cross-correlate these with both the reference and the random samples.

### 2.3 Physical properties of galaxies

The physical quantities necessary for this work include stellar mass  $M_*$ , stellar surface mass density  $\mu_*$ ,  $NUV - r$  colour and colour gradient  $\Delta_{g-i}$ . Stellar masses are derived from SDSS photometry using the methodology described in Salim et al. (2007). These masses are publically available at <http://www.mpa-garching.mpg.de/SDSS/DR7>. The stellar surface mass density is defined as  $\mu_* = M_*/(2\pi R_{50,z}^2)$ , where  $R_{50,z}$  is the physical radius in units of kpc that contains half the total light in the  $z$ -band. The  $NUV$  magnitude is provided by the GALEX pipeline and the  $NUV - r$  colour is corrected for Galactic extinction following Wyder et al. (2007) with  $A_{NUV-r} = 1.9807 A_r$ , where  $A_r$  is the extinction in  $r$ -band derived from the dust maps of Schlegel et al. (1998). The  $g - i$  colour gradient is defined as  $\Delta_{g-i} = (g - i)_{\text{out}} - (g - i)_{\text{in}}$ , where  $(g - i)_{\text{in}}$  and  $(g - i)_{\text{out}}$  are the  $g - i$  colours in the inner and outer regions of the galaxy. The inner region is enclosed by  $R_{50,r}$ , the radius containing half the  $r$ -band light. The outer region is defined as the area between  $R_{50}$  and  $R_{90}$ , the radius enclosing 90 per cent of the  $r$ -band light. A negative value of  $\Delta_{g-i}$  implies that the outer region of the galaxy is *bluer* than the inner region.

### 2.4 Semi-analytic model galaxy catalogues and mock SDSS samples

In this paper we compare our observational results to predictions from the galaxy formation models of G11 and F10. Both models were created by implementing simple prescriptions for baryonic astrophysics on merger trees that follow the evolution of the halo/subhalo population in the Millennium (MS; Springel et al. 2005) Simulation, a cubic region  $500 h^{-1} \text{ Mpc}$  on a side with mass resolution  $\sim 10^{10} M_\odot$ .

The G11 model is the most recent semi-analytic model from the Munich group, in which the treatments of supernova feedback, galaxy size, photoionization suppression and environmental effects on satellite galaxies have been significantly updated. G11 demonstrated that their model provided excellent fits not only to the the luminosity and stellar mass functions of galaxies derived from SDSS data, but also to recent determinations of the abundance of faint satellite galaxies around the Milky Way. The clustering properties of galaxies as a function of stellar mass predicted by the model are in good agreement with SDSS data for masses above  $6 \times 10^{10} M_\odot$  and at separations larger than 2 Mpc. On smaller scales, lower mass galaxies are predicted to be substantially more clustered than observed.

The F10 model is based on an earlier version of the Munich semi-analytic code, which is described in detail in Croton et al. (2006) and updated in De Lucia & Blaizot (2007, hereafter DB07). The main new aspect of this model is that galactic discs are represented by a series of concentric rings in order to track the evolution in the gas and stellar surface density profiles of galaxies over cosmic time. In addition, two simple prescriptions for molecular gas formation processes are included: one is based on the analytic calculations by Krumholz et al. (2009), and one is a prescription

where the  $H_2$  fraction is determined by the pressure of the interstellar medium (Blitz & Rosolowsky 2006). The model is currently being configured to operate on the latest code of G11. The comparison in this paper will be restricted to the model published in the F10 paper and to the  $H_2$  formation prescription of Krumholz et al. (2009).

In this paper, the different treatments of gas stripping in the G11 and F10 models are of interest to us. In most SAMs including DB07, hot gas in a halo is assumed to be stripped immediately after the halo has been accreted on to a larger halo. In the G11 model this prescription has been modified. Satellite galaxies that still are attached to a sub-halo within the larger virialized “parent” halo are still able to accrete gas. This new treatment was motivated by observational findings and hydrodynamical simulations which revealed that the hot atmosphere of massive satellite galaxies may survive for a considerable time after accretion (see G11 and references therein for details). This change primarily affects satellite galaxies located in the outer regions of their host dark matter halos. The timescale for gas to be depleted and star formation to stop becomes significantly longer.

We have constructed a set of 50 mock SDSS galaxy catalogues from the G11 model using both the sky mask and the magnitude and redshift limits of our SDSS reference sample. Detailed description of our methodology can be found in Li et al. (2006b) and Li et al. (2007). These mock catalogues allow us to derive realistic error estimates for the statistics measured below, including both sampling and cosmic variance uncertainties.

### 3 ESTIMATING HI MASS FRACTIONS FOR THE SDSS GALAXIES

There have been a number of attempts to calibrate colours (e.g. Kannappan 2004) or emission-line equivalent widths (e.g. Tremonti et al. 2004; Erb et al. 2006; Bouché et al. 2007) as proxies for the gas-to-stellar mass ratio in galaxies. Zhang et al. (2009) proposed a method motivated by the Kennicutt-Schmidt star formation law (Schmidt 1963; Kennicutt 1998) that combines colour and surface brightness to estimate the  $H_I$ -to-stellar mass ratio. They used a sample of 800 galaxies with  $H_I$  mass measurements from the HyperLeda catalogue (Paturel et al. 2003) and optical photometry from the SDSS to calibrate a relation linking these quantities. In subsequent work, C10 used an unbiased sample of galaxies with  $H_I$  measurements from GASS to show that  $M_{HI}/M_*$  can be well approximated by a linear combination of  $NUV$ -to-optical colour ( $NUV - r$ ) and stellar surface mass density ( $\mu_*$ ) with a  $1\sigma$  scatter of  $\sim 0.3$  dex. However, as could be seen from Figure 12 of C10, galaxies detected by the much shallower ALFALFA survey in redshift range as the GASS sample had significantly higher  $H_I$  mass fractions, and were also systematically displaced from the C10 plane. This result would seem to imply that the  $H_I$  masses of the most gas-rich galaxies in the local Universe cannot be reliably inferred from their UV/optical properties.

However, a recent study by Wang et al. (2011) focusing on the  $H_I$ -rich galaxies from the GASS and ALFALFA samples has revealed that unusually  $H_I$ -rich galaxies have bluer-than-average outer disks. Motivated by this finding,

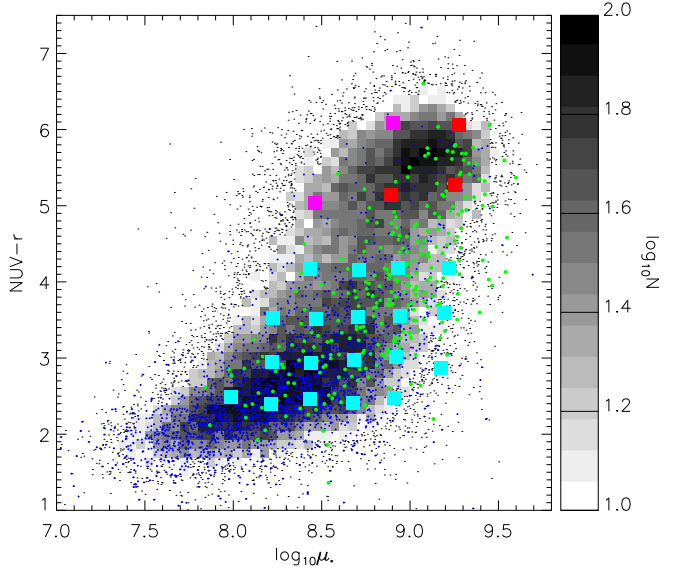


**Figure 1.** Our different galaxy samples in the two dimensional plane of  $NUV-r$  colour and stellar surface mass density. The grey scale indicates the location of the 36,136 galaxies with  $9.5 < \log_{10}(M_*/M_\odot) < 11$  from the SDSS DR7. The green points are GASS galaxies with  $H_I$  detections. The blue points are ALFALFA-detected galaxies in the same redshift range as the GASS sample ( $0.025 < z < 0.05$ ). The squares indicate the grid centers of the  $H_I$  stacking analysis of an optically-selected, volume-limited sample of 5000 galaxies carried out by Fabello et al. (2011). The cyan and red squares indicate the areas of the grid where a high significance measurement of the mean  $H_I$  mass fraction could be obtained from the stacked spectrum. The purple squares indicate the regions where only an upper limit could be derived.

we now propose an updated photometric estimator, that includes both stellar mass and the gradient in  $g - i$  colour as additional parameters.

In Figure 1, we plot some of the galaxy samples we will be working with in this paper in the two dimensional plane of  $NUV - r$  colour and stellar surface mass density. There are 3 grid centers (plotted in red squares) located well within the “red sequence” with good mean  $H_I$  mass measurements and these provide a check on whether our  $H_I$  mass fraction estimators work well in regime where galaxies are gas-poor on average. As can be seen, the combination of the GASS and ALFALFA data, as well as the stacked results, cover the region of  $NUV - r$  versus  $\log_{10} \mu_*$  parameter space reasonably well. The GASS galaxies and stacked results are offset to somewhat higher values of stellar surface mass density, because these samples are restricted to galaxies with stellar masses larger than  $10^{10} M_\odot$ .

Our new estimator is defined by

$$\log_{10} M_{HI}/M_* = a \log_{10} \mu_* + b(NUV - r) + c \log_{10} M_*/M_\odot + d\Delta_{g-i} + e \quad (1)$$

where  $\Delta_{g-i}$  is the colour gradient defined in § 2.3. The coefficients are determined by minimizing the residuals from the plane using the 293  $H_I$  detections in the GASS sample. Following C10, when carrying out the fit, we weight each galaxy by the mass-dependent selection function of the GASS survey. The  $1\sigma$  scatter in our new estimator is 0.31 dex, very



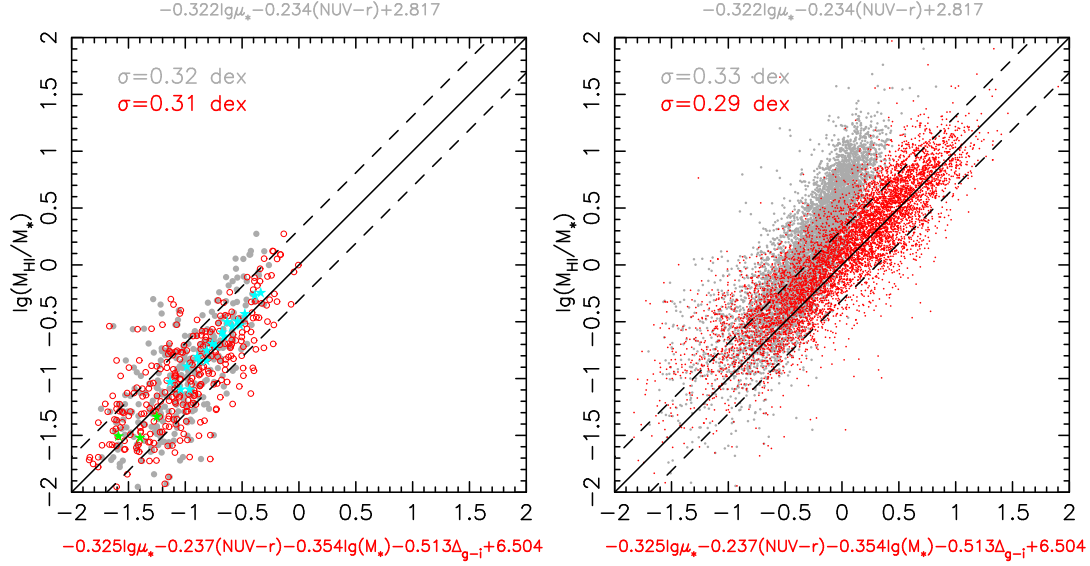


**Figure 2.** In the left-hand panel we plot in red open circles the best-fitting relation between the H I mass fraction ( $M_{\text{HI}}/M_*$ ) and the linear combination of surface mass density  $\mu_*$ ,  $NUV - r$  colour, stellar mass  $M_*$  and the gradient in  $g - i$  colour ( $\Delta_{g-i}$ ) determined from the H I-detected galaxies in the GASS survey. The relation is given in red on the bottom of the panel. This is compared to the grey dots which show the relation obtained by Catinella et al. (2010) between  $M_{\text{HI}}/M_*$  and the linear combination of  $\mu_*$  and  $NUV - r$  (given in grey on the top of the panel). Cyan and green diamonds are results for the stacked spectra (green diamonds are for the 3 stacks on the red sequence). The right-hand panel shows the same thing for a sample of H I-rich galaxies from the ALFALFA survey. The solid and dashed lines in both panels indicate the 1 : 1 relation and  $1\sigma$  error region for the new estimator.

similar to that of the old one. Figure 2 illustrates how this new estimator improves the H I mass fraction estimates.

In the left-hand panel of the figure, grey dots show the H I plane of C10 for GASS galaxies, while coloured stars show the stacked results<sup>1</sup>. In the right-hand panel of the figure, grey dots show the same C10 plane for a sample of  $\sim 7000$  galaxies from the  $\alpha.40$  catalogue of the ALFALFA survey (Haynes et al. 2011) with stellar masses above  $10^8 M_\odot$  and redshifts below 0.06. As can be seen, the majority of the grey points in the right panel lie above the relation.

The H I plane given by the new estimator in equation (1) is plotted in red open circles or red dots in both panels of Figure 2. There is rather little change for the majority of galaxies in the GASS sample. However, the H I-rich galaxies in the ALFALFA sample that were previously displaced to higher-than-predicted H I mass fractions, are now mostly located well within the  $1\sigma$  region of the new relation.

We note that this reduction in the systematic offset for H I-rich galaxies could not be achieved by introducing a single new parameter into the fit (i.e only  $\Delta_{g-i}$ ). Equation (1) implies that the predicted gas fraction scales more strongly with colour gradient in high mass galaxies than in low mass galaxies. The most likely reason for this is that massive galaxies have larger bulge-to-disk ratios than less massive galaxies. Fabello et al. (2011) showed that the H I content of a galaxy did not depend on its bulge-to-disk ratio; the H I mass fraction only depended on the properties of

the disk. It is thus likely that the H I fraction correlates with the colour gradient of the *disk* and the bulge is a contaminant when determining the colour gradient. At present, we do not have bulge/disk decompositions for all the galaxies in our sample, so we do not investigate this hypothesis in more depth. Another effect that may be important is that massive galaxies contain more dust, and this may change the relation between colour gradient and H I fraction.

We now test whether our new estimator exhibits any remaining systematic biases by checking whether the *residuals* are correlated with any intrinsic galaxy property. In Figure 3 we plot the residuals for the C10 estimator (grey dots) and for the new estimator (colourful dots) as a function of  $M_*$ ,  $\mu_*$ ,  $NUV - r$ , and  $R_{90}/R_{50}$ . We only show results for the ALFALFA sample, where the new estimator does change the H I mass fraction predictions by a significant amount.

Figure 3 shows that the new estimator leads to a significant reduction in the large positive residuals for H I rich galaxies with low masses and stellar surface mass densities, blue colours and low concentration indices. The new estimator does not reduce the residuals for galaxies with high stellar surface densities, red colours and high concentration indices. There is still a sub-population of such galaxies that are H I-rich and where equation (1) fails to predict the H I content accurately. An example of such a system is discussed briefly in C10. In addition, one might worry that the H I mass fraction estimation may be biased in this regime, because many red galaxies are not detected in both the GASS and ALFALFA surveys

In the left-hand panel of Figure 2 we plot the results of the H I stacking analysis by Fabello et al. (2011). By stacking samples of a few hundred galaxies, Fabello et al. (2011) were able to estimate mean H I mass fractions for galaxies

<sup>1</sup> Note the bins on the red sequence have been coloured in green and lie very close to an extrapolation of the best-fit line through the other bins, indicating that the C10 plane still yields an accurate prediction of mean H I mass fraction for galaxies on the red sequence

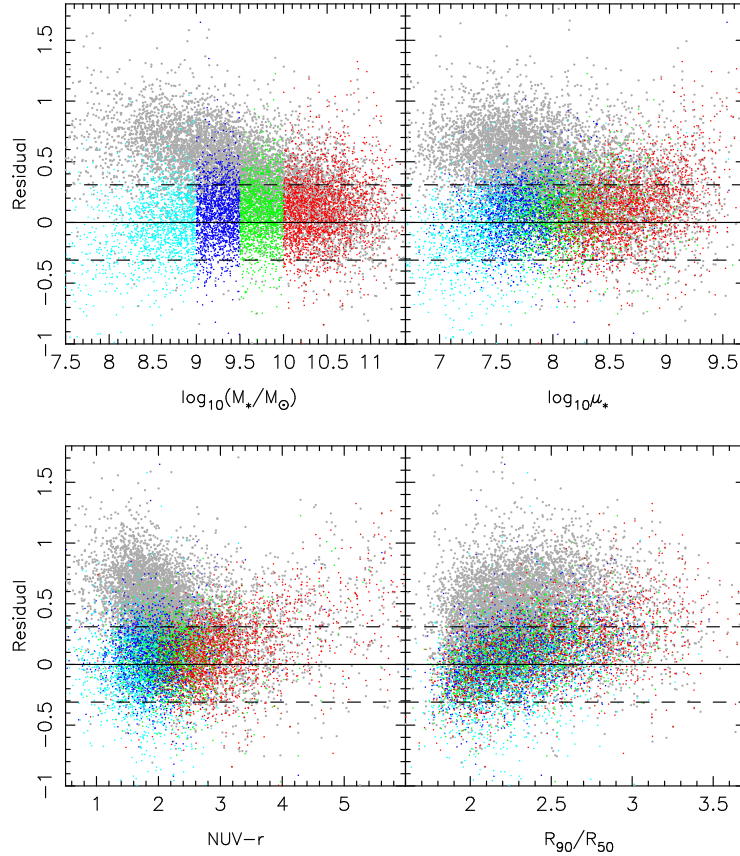


**Figure 3.** Distributions of the residuals in the predicted  $M_{HI}/M_*$  are plotted as functions of stellar mass  $M_*$ , stellar surface mass density  $\mu_*$ ,  $NUV - r$  colour and concentration index  $R_{90}/R_{50}$  for the estimator of Catinella et al. (2010) (grey dots) and for the new estimator in equation (1) (colourful dots). In the latter case the galaxies are divided into four stellar mass intervals and are plotted in different colours (cyan:  $\log_{10}(M_*/M_\odot) < 9$ ; blue:  $9 < \log_{10}(M_*/M_\odot) < 9.5$ ; green:  $9.5 < \log_{10}(M_*/M_\odot) < 10$ ; red:  $\log_{10}(M_*/M_\odot) > 10$ ).

with  $NUV - r$  colours in the range 4 – 6 (shown as green stars on the plot). As can be seen, the C10 estimator accurately reproduces the stacked results with a  $1\sigma$  scatter less than 0.07 dex, even for the reddest stacks. Unfortunately, a similar test is not possible for our new estimator, because the sample of SDSS galaxies with available ALFALFA coverage is too small to carry out a stacking analysis using four different galaxy parameters instead of two. Therefore, in what follows, we divide our galaxies into “red” or “blue” using a mass-dependent colour divider:

$$(NUV - r)_{cut} = 0.5 \log_{10}(M_*/M_\odot) - 1. \quad (2)$$

For “red” galaxies with  $NUV - r > (NUV - r)_{cut}$  we use the old estimator, while the new estimator is applied to “blue” galaxies with  $NUV - r < (NUV - r)_{cut}$ .

We now carry out a test to see whether the estimator introduces any systematic bias in galaxy clustering analyses. We divide all the GASS galaxies including non-detections into six subsamples of equal size, using both the measured value of  $M_{HI}/M_*$  and the predicted value and we compute the projected two-point cross-correlation functions (2PCCF),  $w_p(r_p)$  of these subsamples with the SDSS reference sample. We find that it is very important to take into account the effect of the errors in the predicted value of  $M_{HI}/M_*$  when comparing the results using the photometric estimator with the results using the real HI measurements.

The effect of errors is to weaken the clustering trends as a function of  $M_{HI}/M_*$ , particularly in the tails of the distribution. Here, we model the effect of the errors by adding a random component to the measured value of  $M_{HI}/M_*$  that follows a Gaussian distribution function with a width of 0.31 dex. Results using the measured HI mass fractions convolved with the Gaussian distribution of errors are shown in blue in Figure 4, while results using the photometric estimator are shown in red. The errors in the  $w_p(r_p)$  measurements are computed using the bootstrap resampling technique. The 2PCCF for the whole GASS sample is plotted as a black solid line in each panel for reference. Figure 4 shows that the two  $w_p(r_p)$  calculations agree well with each other. We have repeated the same analysis, using the measured HI mass fraction for the GASS galaxies without including the effect of the errors, and found the results change very little, indicating that the smearing by the HI predictor on the correlation function is sufficiently small.

Although the GASS sample is small, we can still see that both the amplitude and shape of the 2PCCF show strong systematic trends with increasing HI mass fraction. HI-rich galaxies are less strongly clustered on all scales, with more pronounced 1-halo to 2-halo transitions at  $\sim 1$  Mpc. Since galaxy clustering depends on a variety of physical properties, in particular on stellar mass, it is unclear to what extent the

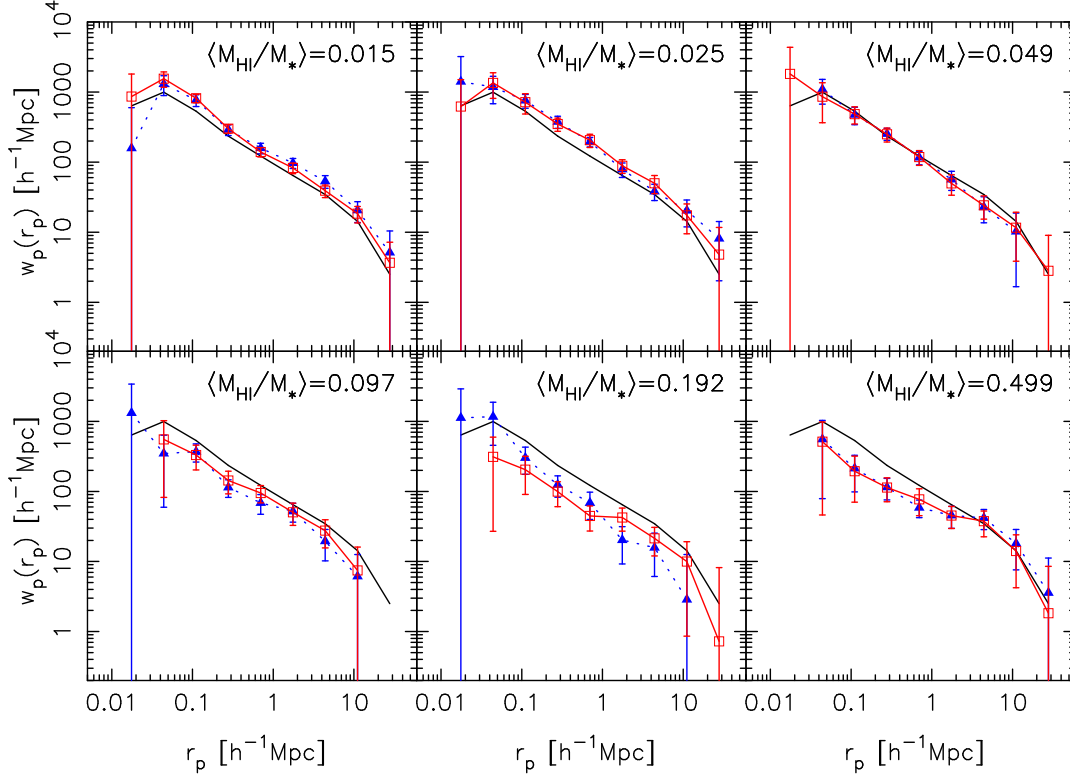


**Figure 4.** Projected two-point cross-correlation function,  $w_p(r_p)$ , for six subsamples with equal number of galaxies from the GASS, selected by the observed HI mass fraction (triangles connected by blue dotted lines) or the predicted value (squares connected by red solid lines). The average value of the HI mass fraction of each subsample is indicated. The result for the whole sample is plotted in the black solid line and repeated in every panel for reference.

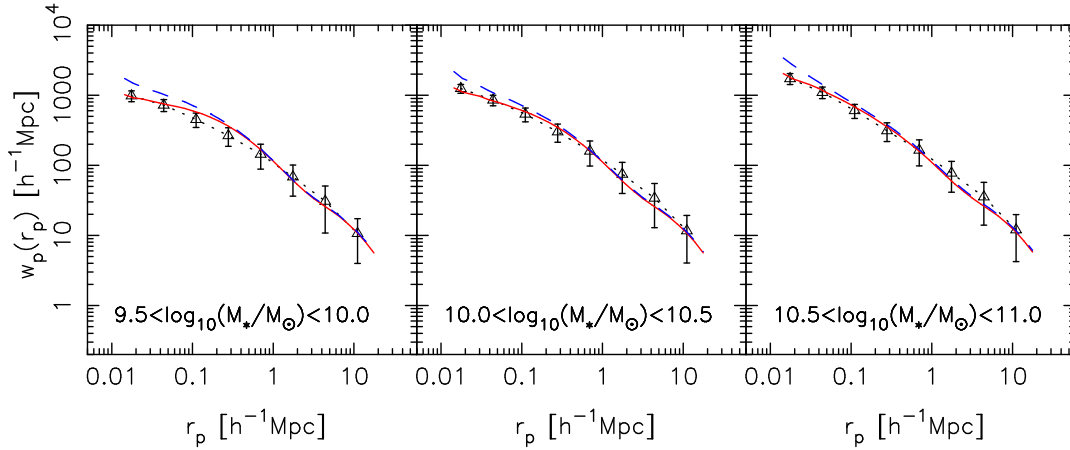


**Figure 6.** The projected two-point cross-correlation function  $w_p(r_p)$  for galaxies in bins of stellar mass with respect to a reference sample of all galaxies. Results for the SDSS DR7 sample are shown in black triangles, while those for the Fu et al. (2010) and Guo et al. (2011) models are shown in red solid lines and in blue dashed lines, respectively. Errors on the SDSS results are estimated from a set of 50 mock galaxy surveys that have the same selection effects as the real SDSS sample.

effect seen from Figure 4 is due to HI content only. We will address this point in the next section.

#### 4 CLUSTERING AS A FUNCTION OF $M_{\text{HI}}/M_*$ AND COMPARISONS WITH SEMI-ANALYTIC MODELS

In this section we apply our new photometric estimator to our full SDSS DR7 galaxy sample to study the dependence of clustering on HI mass fraction. We compare our results with

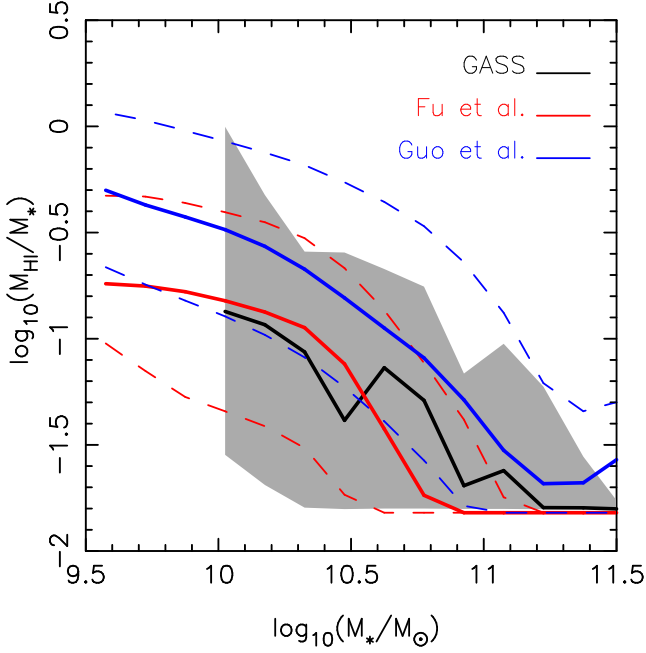


**Figure 5.** Logarithm of the mean HI mass fraction is plotted as a function of the logarithm of the stellar mass for galaxies in the GASS sample (black) and for galaxies in the models of Fu et al. (2010, red) and Guo et al. (2011, blue). The  $1\sigma$  scatter in  $\log_{10}(M_{\text{HI}}/M_*)$  is indicated by the grey shaded area for the data, and by red/blue dashed curves for the models.

predictions from the G11 and F10 models. It is well known that clustering depends strongly on galaxy stellar mass, so the analyses are always carried out in narrow mass intervals. In order to take errors in the photometric estimator into account, we convolve the HI mass fractions predicted by the models with a Gaussian distribution function of width 0.3 dex in  $\log_{10}(M_{\text{HI}}/M_*)$ .

Before we begin, we demonstrate that the models reproduce average trends in HI mass fraction as a function of stellar mass reasonably well. In Figure 5, the black solid curve shows the median value of  $\log_{10} M_{\text{HI}}/M_*$  as a function of stellar mass for galaxies in the GASS survey, while the grey shaded region indicates the 16<sup>th</sup> to 84<sup>th</sup> percentile ranges of  $\log_{10} M_{\text{HI}}/M_*$ . Note that the galaxies without HI line detections are assigned an HI mass equal to the upper limit. This is why the black curve and the shaded region do not fall below  $\log_{10} M_{\text{HI}}/M_* \sim -1.82$  (see C10 for details on the detection limits of the survey). We now perform the same analysis for the simulated galaxies and the results are shown in red and blue for the F10 and G11 models, respectively. We see that the G11 model yields a higher median value of HI gas mass fraction at a given value of  $M_*$ , when compared to both the data and the F10 model.

There are two reasons for this: 1) The G11 model does not account for the partition of the neutral gas into different components. The F10 model includes simple prescriptions for the formation of molecular gas and also properly takes into account the contribution of helium when making predictions for HI content. 2) The F10 model parameters are explicitly adjusted so as to match the HI mass functions determined by existing HI surveys like HIPASS and

ALFALFA. Kauffmann et al. (2012) have shown that the F10 model can also reproduce the distribution of  $M_{\text{HI}}/M_*$  for the population of galaxies with detectable gas, but the model does not provide a fully accurate description of the population of galaxies without detectable cold gas. We note that Figure 5 includes both populations, so the fit to the data is not as good as that shown in Figure 2 of the Kauffmann et al. paper. Since the GASS is a survey only for high mass galaxies with  $\log_{10}(M_*/M_\odot) > 10$ , we are not able to extend this comparison to lower masses. We have compared the models to the data using our *pseudo* HI mass fractions, and this shows that the models roughly match the data at lower masses as well.

Next, Figure 6 demonstrates that both the G11 and F10 models reproduce the observed dependence of  $w_p(r_p)$  on stellar mass. The agreement with observations is equally good for both models on large scales. The F10 model appears to provide a somewhat better fit to the clustering amplitude on scales below  $\sim 1$  Mpc.

In spite of the good agreement as shown above, there still exists discrepancies in some cases. In order to carry out meaningful comparisons between data and models, we order all the galaxies in a given stellar mass range by increasing  $M_{\text{HI}}/M_*$  and divide the galaxies into 10 subsamples, each containing 10 per cent of the whole sample. We analyze the dependence of  $w_p(r_p)$  on HI mass fraction as a function of *HI mass fraction percentile* instead of the absolute value of HI mass fractions<sup>2</sup>. In order to provide a more intuitive feel for our results, we present our measurements in terms of *bias factor*, defined as the ratio of the  $w_p(r_p)$  for a given HI-selected subsample to the  $w_p(r_p)$  of all galaxies in the corresponding stellar mass range. In Figure 7, we plot this bias factor as a function of percentile in  $\log_{10} M_{\text{HI}}/M_*$ , with HI mass fraction increasing from left to right. Results for different intervals in stellar mass are shown in different rows, while results evaluated on different projected scales  $r_p$  are shown in different columns. The data is shown in black curves with shaded regions indicating the  $1\sigma$  errors that are estimated from the bias factor measurements of the 50 mock SDSS catalogues, while the F10 and G11 models are shown in red circles and blue triangles, respectively.

As can be seen, the bias always decreases with increasing HI mass fraction. The trend is strongest for low mass galaxies and on scales of around  $100\text{--}200 h^{-1} \text{ kpc}$ . The agreement between observations and models is good, except for the lowest mass galaxies. For galaxies with stellar masses in the range  $3 \times 10^9 M_\odot$ – $10^{10} M_\odot$ , the observed bias factor drops steeply as a function of HI mass fraction percentile, and then flattens. The bias factor predicted by the models exhibits a more linear trend as a function of HI mass fraction percentile.

As we will now show, this decrease in bias can be understood in a simple way in terms of an increasing ratio of central-to-satellite galaxies as a function of increasing HI mass fraction. To prove that this is the case, we classify each

<sup>2</sup> We note that this only makes sense for the G11 model if the intrinsic scatter in HI-to-H<sub>2</sub> ratio in real galaxies does not change the ranking of  $M_{\text{HI}}/M_*$  with respect to  $[M_{\text{HI}} + M_{\text{H}_2}]/M_*$ . Saintonge et al. (2011) show that the average value of  $M_{\text{HI}}/M_{\text{H}_2}$  is around 1/3 and the molecular gas mass very rarely exceeds the atomic gas mass, so this is likely to be close to correct.



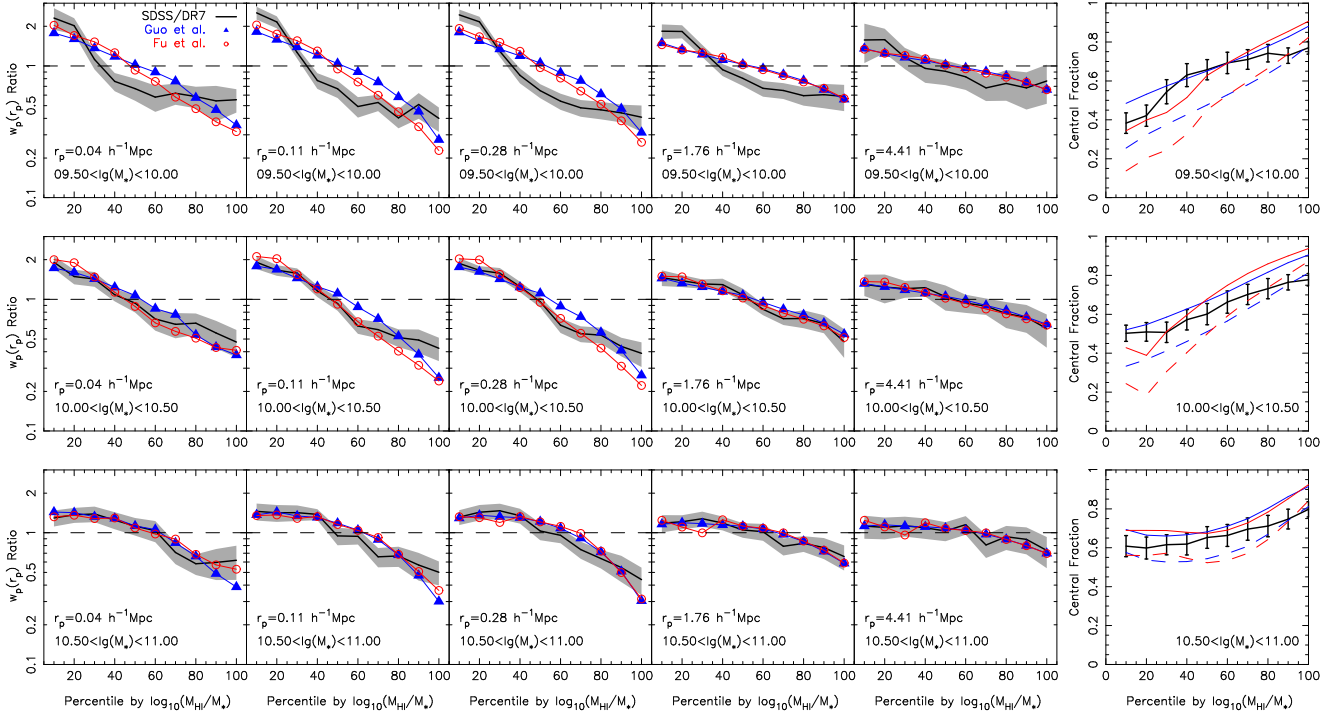


**Figure 7.** Panels on the left-hand side show the clustering bias factor as a function of percentile in  $\log_{10} M_{HI}/M_*$ , at different separations (panels from left to right) and for different stellar mass ranges (panels from top to bottom). The solid line shows observed bias factors, while the shaded region indicate the errors on the observed bias factors estimated from the mock catalogues. Model results are shown in red/blue for the F10/G11 models. In the right-most column, the central galaxy fraction is plotted as a function of percentile in  $\log_{10} M_{HI}/M_*$ . The black curves with error bars show the central fractions estimated from the data (see text). The dashed red/blue curves show the true central fractions from the models. The solid red/blue curves show the central fractions in the models when estimated in the same way as in the data.

galaxy in our sample as either a central galaxy or a satellite galaxy based on whether it is more massive than all companions within a cylinder with projected radius  $R_{max}$  and a line-of-sight depth of  $\pm 1000 \text{ km s}^{-1}$ . Here,  $R_{max}$  is set to twice the virial radius of the host dark matter halo of the galaxy. We have adopted the stellar mass-halo mass relation derived by Guo et al. (2010) to estimate a halo mass for the galaxy, and then estimate a ‘virial’ radius of the halo using the model of Eke et al. (2001). In addition, we require that a central galaxy should not fall within  $R_{max}$  of any other more massive galaxy.

In the right-hand panels in Figure 7, we plot the fraction of central galaxies,  $f_{cen}$ , as a function of H I fraction percentile (the black solid line). We see that  $f_{cen}$  increases with increasing H I content, with the effect stronger at low stellar masses.

We can of course check whether the models predict a similar increase in  $f_{cen}$  as a function of H I gas fraction. In the right column of Figure 7, the dashed curves show the *true* values of  $f_{cen}$  as a function of H I fraction percentile for the F10 (red) and G11 (blue) models. The central fractions in the F10 model are lower than those in the G11 model at low H I mass fractions, particularly for galaxies with low stellar masses. This reflects the fact that gas consumption times in satellite galaxies are longer in the G11 model than in the F10 model.

In order to make a fair comparison with observations, we have also computed  $f_{cen}$  for the model galaxies in exactly

the same way as in the observations. In brief, we project the model galaxies onto the  $x - y$  plane and take the  $z$ -axis as the line-of-sight direction (i.e. we adopt the distant observer approximation). We then apply exactly the same procedure described above to classify each galaxy as central or satellite. The  $z$ -axis peculiar velocities of the galaxies are added to their  $z$ -axis positions. In addition, halo masses and virial radii are not taken from the model catalogue, but are estimated exactly the same way as for the observational data. Results are plotted as solid red and blue curves in the right-hand panels of Figure 7.

We note that the true central fractions are always smaller than the ones that use a classification technique based on whether or not brighter companions are found in cylinders around the galaxy. However, our classification technique preserves the shape of the relation between central fraction and H I gas fraction percentile, as well as the differences between the F10 and G11 models. We also see that the central fractions estimated in cylinders in the simulation agree reasonably well with the data. As was the case for the bias factor, the behaviour of the central fraction as function of H I mass fraction percentile in the models is somewhat different to what is seen in the observations, particularly at low stellar masses.

In summary, the general agreement with the models supports our conjecture that the trends in bias factor as a function of H I mass fraction mainly arise as a result of trends in the satellite-to-central ratio.

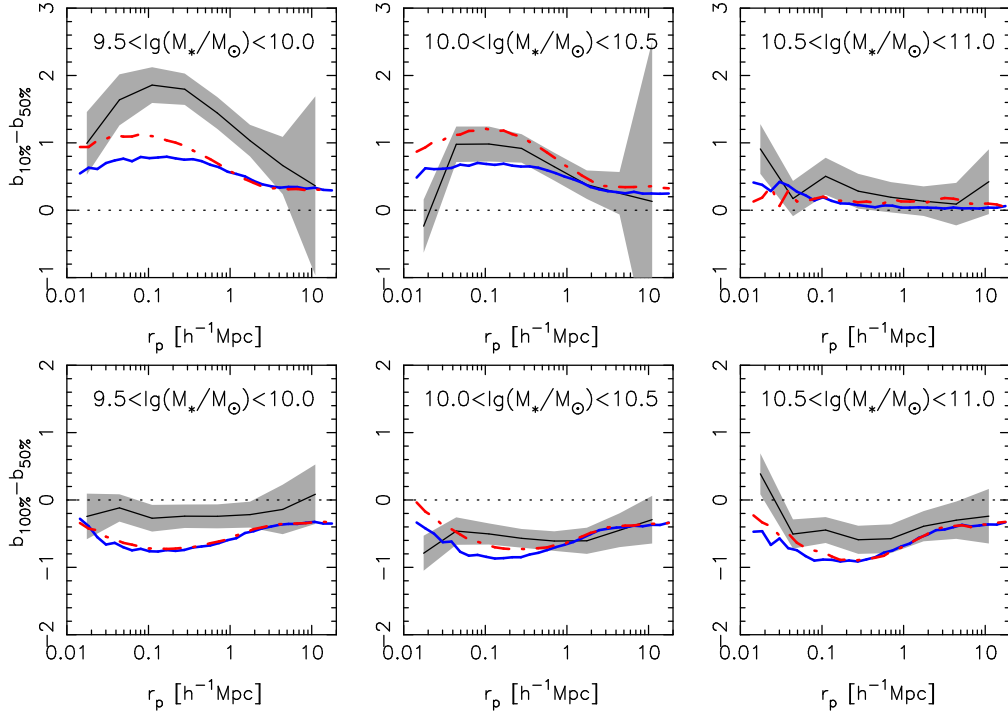


**Figure 8.** In the upper panels, we plot the change in bias factor from the 10<sup>th</sup> percentile to the 50<sup>th</sup> percentile in  $\log_{10}(M_{HI}/M_*)$  as a function of projected physical scale, for different stellar mass intervals as indicated. The black line shows the result from the SDSS/DR7. The errors estimated from the mock catalogues are shown as shaded regions. The red dotted-dashed line and the blue solid line show results from the Fu et al. (2010) and Guo et al. (2011) models after convolution with errors. The lower panels show the change in bias factor from the 50<sup>th</sup> to the 100<sup>th</sup> percentile.

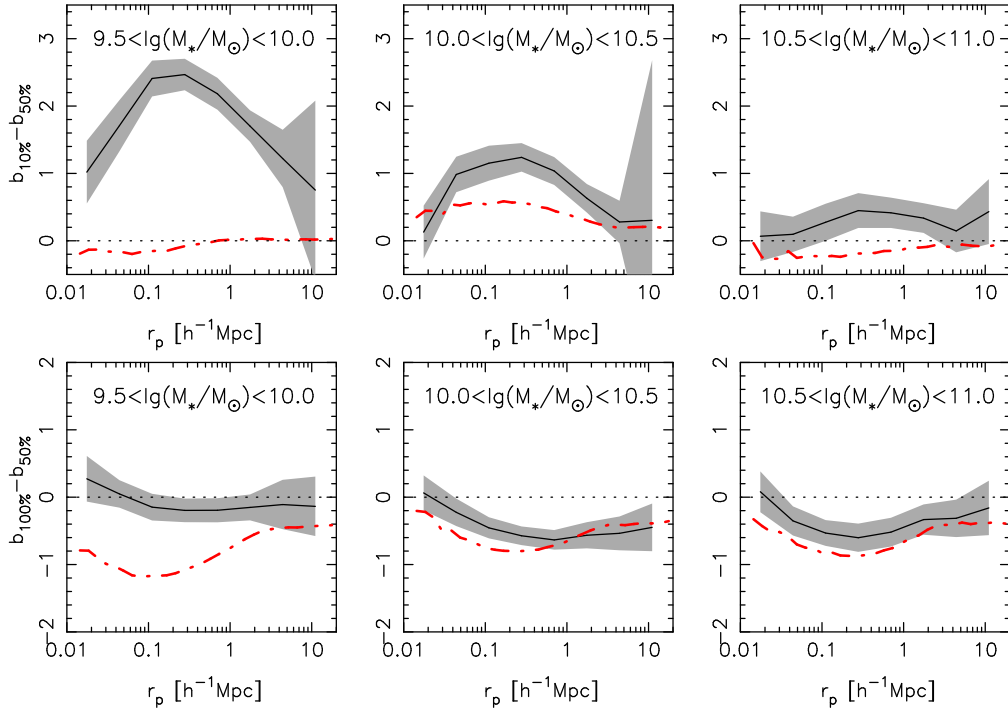


**Figure 9.** Same as the previous figure, except that the galaxies are ordered by the deviation in  $\log_{10}(M_{HI}/M_*)$  from the value predicted from the mean relation between  $\log_{10}(M_{HI}/M_*)$  and galaxy mass  $M_*$  and stellar surface mass density  $\mu_*$ . Red dotted-dashed curves show results from the model of Fu et al. (2010) after convolution with errors.

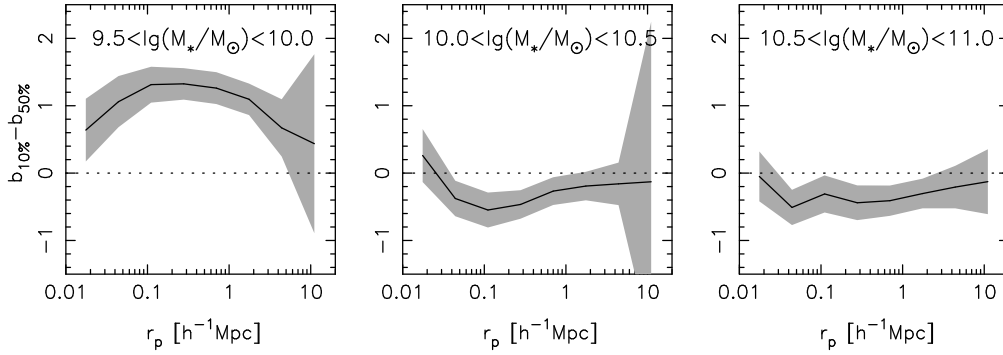


**Figure 10.** Same as the bottom panel of the previous figure, except that the galaxies are ordered by the deviation in  $\log_{10}(M_{\text{HI}}/M_*)$  from the value predicted from the mean relation between  $\log_{10}(M_{\text{HI}}/M_*)$  and galaxy mass  $M_*$ , stellar surface mass density  $\mu_*$ , and  $NUV - r$  colour.

## 5 SCALE DEPENDENCE OF THE BIAS FOR GALAXIES WITH EXCESS/DEFICIENT HI CONTENT

In the previous section, we studied how the bias factor changes as a function of normalized HI mass fraction for galaxies in different stellar mass bins. The results presented in Figure 7 clearly show that the change in the bias factor between “gas-poor” and “gas-rich” galaxies depends on scale  $r_p$ .

In this section, we analyze the scale-dependence of the *change* in bias factor for both gas-deficient and gas-rich galaxies. We note that Haynes & Giovanelli (1984) defined gas-deficiency to be the difference in HI content between cluster galaxies and “field” galaxies of the same morphological type and size. There are some difficulties with this definition, including the definition of “field” and the fact that Hubble classification is problematic in rich clusters. Some more recent analyses have used a type-independent deficiency parameter that compares all galaxies to a fixed HI surface density (Chung et al. 2009). One worry with this, is that the mean HI content of galaxies scales strongly with galaxy parameters such as stellar mass and surface density (Catinella et al. 2010).

In this analysis, we will adopt a flexible approach to defining “pseudo” HI deficiency parameters. We will analyze the photometrically-predicted HI content with respect to galaxies of the same stellar mass, with respect to galaxies of the same mass and size, and with respect to galaxies of the same mass, size and colour (as in Cortese et al. 2011).

In the upper panels of Figure 8, we show the change in bias factor between the 10<sup>th</sup> and 50<sup>th</sup> percentile bins in  $\log_{10} M_{\text{HI}}/M_*$ . This serves as a test of gas-stripping mechanisms in gas-deficient galaxies. The lower panels show the change in bias factor between the 100<sup>th</sup> and 50<sup>th</sup> percentile bins in  $\log_{10} M_{\text{HI}}/M_*$ . This serves as a test of gas accretion mechanisms in gas-rich galaxies.

Results for the SDSS DR7 galaxies are shown as black curves in Figure 8. Grey shaded regions indicate the  $1\sigma$  errors on our estimates, obtained from the 50 mock SDSS catalogues. Results for the F10 and G11 models are shown as red and blue curves and we plot our results in three different stellar mass ranges. As can be seen from the plot, the change in bias factor between gas-deficient galaxies and

galaxies with typical gas fractions is most pronounced for low stellar mass systems. The bias factor difference peaks at relatively small physical scales ( $\sim 100 - 300$  kpc). For the most massive galaxies with  $10.5 < \log_{10}(M_*/M_\odot) < 11$ , there is little change in bias on any scale. For galaxies with  $9.5 < \log_{10}(M_*/M_\odot) < 10$ , the increase in clustering amplitude from galaxies with typical gas mass fractions to the most gas-deficient objects reaches a factor of 2 on scales of a few hundred kpc. On scales larger than  $2 - 3$  Mpc, there is no significant change in clustering amplitude. The results are consistent with the idea that gas quenching is driven by processes that are *internal* to dark matter halos. The models agree well with the data at stellar masses greater than  $10^{10} M_\odot$ , but at lower stellar masses the models predict a weaker bias for gas-deficient galaxies than is actually seen.

As seen in the bottom panels of Figure 8, the change in bias factor between very gas-rich galaxies and galaxies with typical gas fractions appears to be weaker rather than stronger at low stellar masses. The most gas-rich galaxies with stellar masses greater than  $10^{10} M_\odot$  are more weakly clustered than galaxies with typical gas fractions, indicating that they occupy lower mass dark matter halos on average. At stellar masses below  $10^{10} M_\odot$ , there is no anti-bias of gas-rich galaxies seen in the data. However, the models do predict clear anti-bias effects.

One might question whether ranking galaxies by HI mass fraction is sufficient to characterize whether a galaxy is classified as gas-rich or gas-deficient. As discussed in § 3, galaxies of fixed stellar mass and colour have higher HI mass fractions if they have larger sizes (i.e. lower stellar surface mass densities). One way to understand this is to appeal to standard disk formation models (e.g. F10; Kauffmann 1996; Mo et al. 1998). In these models, the spin parameter of the dark matter halo determines the contraction factor of the infalling gas. Larger disks in a dark matter halo of fixed mass will have higher HI mass fractions because gas surface densities are low and gas consumption times are long. In this case, it would make more sense to define galaxies as gas-rich or gas-deficient by comparing their HI mass fractions to other galaxies of the same *mass and size*.

One might also consider an even more stringent constraint that HI-rich/HI-deficient galaxies be classified as those objects with higher/lower-than-average HI content given their stellar mass, size and star formation rate. This

might indicate that the galaxy has experienced a recent gas accretion episode and that the *global* star formation has not yet had a chance to respond to the extra fuel supply. In our scheme of using photometric quantities to predict HI content, the HI-rich systems would correspond to those galaxies with bluer-than-average outer disks. Recall that the HI content in gas-poor regime is currently calibrated using only stellar surface density and colour; we therefore do not delve into the opposite regime, where gas has been recently removed from a galaxy.

In Figures 9 and 10 we investigate clustering trends using these alternative definitions. For Figure 9, we rank galaxies as a function of their deviation from the average HI mass fraction of all galaxies of the same stellar mass ( $M_*$ ) and stellar surface mass density ( $\mu_*$ ). As seen from equation (1), this deviation depends on both the  $NUV - r$  colour of the galaxy and its  $g - i$  colour gradient. For Figure 10, we rank galaxies as a function of their deviation from the average HI mass fraction of all galaxies of the same  $M_*$ ,  $\mu_*$  and  $NUV - r$ . This then depends only on the  $g - i$  colour gradient of the galaxy.

Interestingly, the top panels of Figure 9 show that when gas deficiency is expressed relative to galaxies of the same stellar mass and size, the change in bias on scales between a few hundred kpc and 1 Mpc becomes much more pronounced. The change in bias factor for the lowest mass galaxies now reaches values near  $\sim 3$  and even massive gas-deficient galaxies are now significantly biased with respect to their counterparts with “normal” gas fractions.

The F10 model provides predictions of the radial profiles of the gas and the stars in galaxies. It is thus possible to look at gas deficiency at fixed mass and stellar surface density in the model. Results are plotted as red curves in Figure 9. We see that the model disagrees very strongly with the observations. In the model, bias effects become *weaker rather than stronger* when gas deficiency is defined with respect to galaxies of the same mass and size. These results would appear to suggest that in the real Universe, gas removal processes depend on the size/density of the galaxy itself. This is not the case in the models, where satellite galaxies become gas-poor only because their supply of infalling gas has been cut off. Thus the data suggest that processes such as ram-pressure stripping, which depend on the density of the interstellar medium (ISM), may play an important part in explaining the observed trends.

In contrast to what is seen for gas-deficient galaxies, if gas-richness is normalized with respect to galaxies of the same stellar mass and size, the bias trends remain much the same and the F10 model predictions still fit reasonably well for galaxies more massive than  $10^{10} M_\odot$ . This suggests that gas accretion processes are being modelled quite successfully at high stellar masses.

Figure 10 shows that the bias effects for gas-rich galaxies are still roughly of the same strength as in the previous figure, when gas-richness is expressed relative to galaxies of the same mass, size and global  $NUV - r$  colour. This means that the clustering does depend strongly on the colour-gradient term for these objects. Galaxies with bluer-than-average outer colours are clearly located in lower-density environments compared to galaxies where there is no evidence for younger-than-average stellar populations in the outer disk.

## 6 SUMMARY AND DISCUSSION

We introduce a new photometric estimator for estimating the HI mass fraction ( $M_{HI}/M_*$ ) in local galaxies. The estimator is calibrated with a sample of 293 galaxies with  $M_* > 10^{10} M_\odot$  in the redshift range  $0.025 < z < 0.05$ , which are detected in HI emission line by the GASS survey. The estimator is a linear combination of four parameters: stellar mass  $M_*$ , stellar surface mass density  $\mu_*$ , near-UV-to-optical colour  $NUV - r$ , and the gradient in  $g - i$  colour  $\Delta_{g-i}$ . We demonstrate that this estimator provides unbiased  $M_{HI}/M_*$  estimates for HI-rich galaxies.

We then apply this estimator to a sample of  $\sim 24,000$  galaxies from the SDSS/DR7 that lie in the same redshift range. We analyze the clustering of these galaxies as a function of stellar mass and as a function of HI mass fraction  $M_{HI}/M_*$  and we compare the results with predictions from two recent semi-analytic models of galaxy formation by Fu et al. (2010) and Guo et al. (2011). Our results may be summarized as follows:

- Clustering depends strongly on HI mass fraction at fixed  $M_*$ . Galaxies with large values of  $M_{HI}/M_*$  are more weakly clustered. The total change with HI mass fraction in clustering strength is largest for low mass galaxies,
- At fixed  $M_*$ , the clustering dependence on HI mass fraction is strongest on scales of a few hundred kpc. On large scales ( $> 1$  Mpc), clustering depends weakly on HI mass fraction. This suggests the HI content of a galaxy of fixed stellar mass depends on location within its dark matter halo.
- After the uncertainty in the HI mass fraction estimator is taken into account, the observed dependence of clustering on HI mass fraction is well reproduced by the models for galaxies more massive than  $10^{10} M_\odot$ . Significant discrepancies remain at lower stellar masses.

In the next part of the paper, we extend the analysis by studying the clustering of HI-deficient and HI-rich galaxies defined in two ways: 1) with respect to the average HI content of galaxies of the same stellar mass and size, 2) with respect to the average HI content of galaxies of the same stellar mass, size and  $NUV - r$  colour. These definitions are motivated by the following considerations. First, models in which disks form from gas that cools and condenses in dark matter halos, while conserving angular momentum, predict that the gas fractions of equilibrium disks depend on both their mass and their size. Second, the majority of nearby spiral galaxies are *observed* to lie on a relatively tight plane linking HI gas mass fraction with stellar mass, stellar surface density and  $NUV - r$  colour (Catinella et al. 2010). It is natural to suppose that galaxies that have undergone a recent gas accretion event would be displaced to higher HI mass fractions with respect to this plane. Conversely, galaxies that have been stripped of their gas would be displaced to lower values of  $M_{HI}/M_*$ .

The main results of our analysis of HI-rich and HI-deficient galaxies can be summarized as follows.

- When HI deficiency is defined with respect to galaxies of the same stellar mass and size, the bias of HI-deficient galaxies relative to normal galaxies is larger than obtained if the HI deficiency is defined with respect to galaxies of the same mass. The same effect is not reproduced in the semi-analytic model of Fu et al. (2010).



• When H I-richness is expressed with respect to galaxies of the same mass and size (as well as with respect to galaxies of the same mass, size and colour), H I-rich galaxies more massive than  $10^{10} M_{\odot}$  are observed to be anti-biased with respect to their counterparts with normal H I content. The same is not true at lower stellar masses.

We have proposed that the disagreement between the observations and the models might be resolved, if processes such as ram-pressure stripping, which depend on the density of the ISM, are included in the models. We note that the lowest mass galaxies have the lowest densities and are thus the most likely to be affected by ram-pressure. In order to test this hypothesis in more detail, we plan to look behaviour of gas deficiency as a function of cluster-centric radius in samples of nearby groups and clusters.

We also stress that next generation wide-field H I surveys such as the ASKAP H I All-sky Survey (WALLABY) and surveys carried out by the Apertif receiver array on the Westerbork Synthesis Radio Telescope will measure H I masses and sizes for samples of tens to hundreds of thousands of galaxies at redshifts of around 0.1. These surveys will make it possible to investigate clustering as a function of the true H I content of a galaxy. It will be interesting to investigate the degree to which the results conform with our current analysis of “pseudo” H I content. Discrepancies may reveal additional physics that we have not yet considered. In the meantime, the construction of models that can reproduce the gas properties of galaxies as well as possible, is an important step towards building mock surveys that can be safely used for making predictions in support of these surveys.

## ACKNOWLEDGMENTS

CL thanks the Max-Planck Institute for Astrophysics (MPA) for warm hospitality while this work was being completed. This work is sponsored by NSFC (no. 11173045), Shanghai Pujiang Program (no. 11PJ1411600) and the CAS/SAFEA International Partnership Program for Creative Research Teams (KJCX2-YW-T23). CL acknowledges the support of the 100 Talents Program of Chinese Academy of Sciences (CAS) and the exchange program between Max Planck Society and CAS.

Funding for the SDSS and SDSS-II has been provided by the Alfred P. Sloan Foundation, the Participating Institutions, the National Science Foundation, the U.S. Department of Energy, the National Aeronautics and Space Administration, the Japanese Monbukagakusho, the Max Planck Society, and the Higher Education Funding Council for England. The SDSS Web Site is <http://www.sdss.org/>. The SDSS is managed by the Astrophysical Research Consortium for the Participating Institutions. The Participating Institutions are the American Museum of Natural History, Astrophysical Institute Potsdam, University of Basel, University of Cambridge, Case Western Reserve University, University of Chicago, Drexel University, Fermilab, the Institute for Advanced Study, the Japan Participation Group, Johns Hopkins University, the Joint Institute for Nuclear Astrophysics, the Kavli Institute for Particle Astrophysics and Cosmology, the Korean Scientist Group, the

Chinese Academy of Sciences (LAMOST), Los Alamos National Laboratory, the Max-Planck-Institute for Astronomy (MPIA), the Max-Planck-Institute for Astrophysics (MPA), New Mexico State University, Ohio State University, University of Pittsburgh, University of Portsmouth, Princeton University, the United States Naval Observatory, and the University of Washington.

## REFERENCES

- Abazajian K. N., Adelman-McCarthy J. K., Agüeros M. A., Allam S. S., Allende Prieto C., An D., Anderson K. S. J., Anderson S. F., et al., 2009, *ApJS*, 182, 543
- Adelman-McCarthy J. K., Agüeros M. A., Allam S. S., Allende Prieto C., Anderson K. S. J., Anderson S. F., Annis J., Bahcall N. A., et al., 2008, *ApJS*, 175, 297
- Benson A. J., Cole S., Frenk C. S., Baugh C. M., Lacey C. G., 2000, *MNRAS*, 311, 793
- Blitz L., Rosolowsky E., 2006, *ApJ*, 650, 933
- Bouché N., Cresci G., Davies R., Eisenhauer F., Förster Schreiber N. M., Genzel R., Gillessen S., Lehnert M., et al., 2007, *ApJ*, 671, 303
- Bower R. G., Benson A. J., Malbon R., Helly J. C., Frenk C. S., Baugh C. M., Cole S., Lacey C. G., 2006, *MNRAS*, 370, 645
- Catinella B., Kauffmann G., Schiminovich D., Lemonias J., Scannapieco C., Wang J., Fabello S., Hummels C., et al., 2011, *ArXiv e-prints*
- Catinella B., Schiminovich D., Kauffmann G., Fabello S., Wang J., Hummels C., Lemonias J., Moran S. M., et al., 2010, *MNRAS*, 403, 683
- Chung A., van Gorkom J. H., Kenney J. D. P., Crowl H., Vollmer B., 2009, *AJ*, 138, 1741
- Cole S., Aragon-Salamanca A., Frenk C. S., Navarro J. F., Zepf S. E., 1994, *MNRAS*, 271, 781
- Colless M., Dalton G., Maddox S., Sutherland W., Norberg P., Cole S., Bland-Hawthorn J., Bridges T., et al., 2001, *MNRAS*, 328, 1039
- Cortese L., Catinella B., Boissier S., Boselli A., Heinis S., 2011, *MNRAS*, 415, 1797
- Croton D. J., Springel V., White S. D. M., De Lucia G., Frenk C. S., Gao L., Jenkins A., Kauffmann G., et al., 2006, *MNRAS*, 365, 11
- De Lucia G., Blaizot J., 2007, *MNRAS*, 375, 2
- Eisenstein D. J., Zehavi I., Hogg D. W., Scoccimarro R., Blanton M. R., Nichol R. C., Scranton R., Seo H.-J., et al., 2005, *ApJ*, 633, 560
- Eke V. R., Navarro J. F., Steinmetz M., 2001, *ApJ*, 554, 114
- Erb D. K., Steidel C. C., Shapley A. E., Pettini M., Reddy N. A., Adelberger K. L., 2006, *ApJ*, 646, 107
- Fabello S., Catinella B., Giovanelli R., Kauffmann G., Haynes M. P., Heckman T. M., Schiminovich D., 2011, *MNRAS*, 411, 993
- Fu J., Guo Q., Kauffmann G., Krumholz M. R., 2010, *MNRAS*, 409, 515
- Giovanelli R., Haynes M. P., Kent B. R., Perillat P., Sain- tonge A., Brosch N., Catinella B., Hoffman G. L., et al., 2005, *AJ*, 130, 2598

- Guo Q., White S., Boylan-Kolchin M., De Lucia G., Kauffmann G., Lemson G., Li C., Springel V., et al., 2011, *MNRAS*, 413, 101
- Guo Q., White S., Li C., Boylan-Kolchin M., 2010, *MNRAS*, 404, 1111
- Haynes M. P., Giovanelli R., 1984, *AJ*, 89, 758
- Haynes M. P., Giovanelli R., Martin A. M., Hess K. M., Saintonge A., Adams E. A. K., Hallenbeck G., Hoffman G. L., et al., 2011, *AJ*, 142, 170
- Kannappan S. J., 2004, *ApJ*, 611, L89
- Kauffmann G., 1996, *MNRAS*, 281, 475
- Kauffmann G., Li C., Fu J., Saintonge A., Catinella B., Tacconi L. J., Kramer C., Genzel R., et al., 2012, *MNRAS*, 2601
- Kauffmann G., White S. D. M., Guiderdoni B., 1993, *MNRAS*, 264, 201
- Kennicutt Jr. R. C., 1998, *ARA&A*, 36, 189
- Kim H.-S., Baugh C. M., Benson A. J., Cole S., Frenk C. S., Lacey C. G., Power C., Schneider M., 2011, *MNRAS*, 414, 2367
- Krumholz M. R., McKee C. F., Tumlinson J., 2009, *ApJ*, 699, 850
- Li C., Jing Y. P., Kauffmann G., Börner G., Kang X., Wang L., 2007, *MNRAS*, 376, 984
- Li C., Kauffmann G., Heckman T. M., White S. D. M., Jing Y. P., 2008, *MNRAS*, 385, 1915
- Li C., Kauffmann G., Jing Y. P., White S. D. M., Börner G., Cheng F. Z., 2006a, *MNRAS*, 368, 21
- Li C., Kauffmann G., Wang L., White S. D. M., Heckman T. M., Jing Y. P., 2006b, *MNRAS*, 373, 457
- Li C., White S. D. M., Chen Y., Coil A. L., Davis M., De Lucia G., Guo Q., Jing Y. P., et al., 2012, *MNRAS*, 419, 1557
- Martin D. C., Fanson J., Schiminovich D., Morrissey P., Friedman P. G., Barlow T. A., Conrow T., Grange R., et al., 2005, *ApJ*, 619, L1
- Meyer M. J., Zwaan M. A., Webster R. L., Brown M. J. I., Staveley-Smith L., 2007, *ApJ*, 654, 702
- Mo H. J., Mao S., White S. D. M., 1998, *MNRAS*, 295, 319
- Passmoor S. S., Cress C. M., Faltenbacher A., 2011, *ArXiv e-prints*
- Paturel G., Theureau G., Bottinelli L., Gouguenheim L., Coudreau-Durand N., Hallet N., Petit C., 2003, *A&A*, 412, 57
- Peacock J. A., Smith R. E., 2000, *MNRAS*, 318, 1144
- Popping A., Davé R., Braun R., Oppenheimer B. D., 2009, *A&A*, 504, 15
- Saintonge A., Kauffmann G., Wang J., Kramer C., Tacconi L. J., Buchbender C., Catinella B., Graciá-Carpio J., et al., 2011, *MNRAS*, 415, 61
- Salim S., Rich R. M., Charlot S., Brinchmann J., Johnson B. D., Schiminovich D., Seibert M., Mallery R., et al., 2007, *ApJS*, 173, 267
- Schiminovich D., Catinella B., Kauffmann G., Fabello S., Wang J., Hummels C., Lemonias J., Moran S. M., et al., 2010, *MNRAS*, 408, 919
- Schlegel D. J., Finkbeiner D. P., Davis M., 1998, *ApJ*, 500, 525
- Schmidt M., 1963, *ApJ*, 137, 758
- Spergel D. N., Verde L., Peiris H. V., Komatsu E., Nolte M. R., Bennett C. L., Halpern M., Hinshaw G., et al., 2003, *ApJS*, 148, 175
- Springel V., White S. D. M., Jenkins A., Frenk C. S., Yoshida N., Gao L., Navarro J., Thacker R., et al., 2005, *Nature*, 435, 629
- Tegmark M., Strauss M. A., Blanton M. R., Abazajian K., Dodelson S., Sandvik H., Wang X., Weinberg D. H., et al., 2004, *Phys.Rev.D*, 69, 103501
- Tremonti C. A., Heckman T. M., Kauffmann G., Brinchmann J., Charlot S., White S. D. M., Seibert M., Peng E. W., et al., 2004, *ApJ*, 613, 898
- Wang J., Kauffmann G., Overzier R., Catinella B., Schiminovich D., Heckman T. M., Moran S. M., Haynes M. P., et al., 2011, *MNRAS*, 412, 1081
- Wyder T. K., Martin D. C., Schiminovich D., Seibert M., Budavári T., Treyer M. A., Barlow T. A., Forster K., et al., 2007, *ApJS*, 173, 293
- York D. G., Adelman J., Anderson Jr. J. E., Anderson S. F., Annis J., Bahcall N. A., Bakken J. A., Barkhouser R., et al., 2000, *AJ*, 120, 1579
- Zhang W., Li C., Kauffmann G., Zou H., Catinella B., Shen S., Guo Q., Chang R., 2009, *MNRAS*, 397, 1243
- Zwaan M. A., Meyer M. J., Staveley-Smith L., Webster R. L., 2005, *MNRAS*, 359, L30

This paper has been typeset from a  $\text{\LaTeX}$  file prepared by the author.